Available online at www.sciencedirect.com
ScienceDirect
Journal of Sound and Vibration 323 (2009) 33–50
JOURNAL OF SOUND AND VIBRATION
www.elsevier.com/locate/jsvi

# Using passively shunted electromechanical transducers to control the boundary impedance of dynamic test fixtures

Timothy S. Edwards*

*Sandia National Laboratories[1], MS0346, P.O. Box 5800, Albuquerque, NM 87185, USA*

Received 20 August 2008; received in revised form 25 November 2008; accepted 4 December 2008
Handling Editor: S. Bolton
Available online 18 January 2009

**Abstract**

One of the most basic problems with testing components in the vibration laboratory involves the discrepancy in boundary conditions between the laboratory and field environments. Boundary impedances that a component experiences when mounted in the field are usually quite different from those of traditional vibration test fixtures. These discrepancies can have dramatic effects on component response and therefore, the outcome of the vibration test. Simulation of field boundary conditions can be difficult because of the stochastic and time varying nature of some boundary impedances. A test fixture whose impedance can be continuously varied would be valuable in both qualification and modal-type testing. Similarly, a device that could mimic component impedance for purposes of test machine calibration would be of significant value. This paper develops the concepts necessary to implement variable impedance devices using electrically shunted piezoelectric and magnetostrictive transducers. Linear transducer models are developed and validated through experimentation. Practical considerations such as nonlinear transducer behavior are discussed.


## 1. Introduction

The accurate simulation of the shock and vibration environments is of great interest at Sandia National Laboratories. Of particular interest is the simulation of these environments for components of larger, complex systems. When a component is removed from a larger system for testing, attention must be given to the impedance[2] of the boundary conditions at both the system level and during the component-level test to ensure that the test objectives are met [1].

The response of components under dynamic loading can be quite sensitive to the boundary conditions imposed. Input forces, failure modes and force-response relationships are all affected by the boundary

*Tel.: +1 505 844 0044.
*E-mail address:* tsedwar@sandia.gov

[1]Sandia is a multiprogram laboratory operated by Sandia Corporation, a Lockheed Martin Company, for the United States Department of Energy's National Nuclear Security Administration under Contract DE-AC04-94AL85000.

[2]In mechanical systems the term "impedance" strictly refers to the complex ratio of output force to input velocity as a function of frequency. With a slight abuse of terminology, in this work the term impedance is loosely taken to mean any of the various input–output relations.

0022-460X/$ - see front matter © 2008 Elsevier Ltd. All rights reserved.
doi:10.1016/j.jsv.2008.12.011

**Nomenclature**

| | |
|---|---|
| $A$ | area |
| $B$ | magnetic flux intensity |
| $C_i$ | capacitance of shunt circuit (F) |
| $C_p$ | capacitance of piezoelectric transducer (F) |
| $D$ | electrical displacement (Coulombs/m$^2$) |
| $d$ | piezoelectric charge constant (Coulombs/N) |
| $E$ | electric field (V/m) |
| $F$ | force |
| $H$ | magnetic field |
| $I$ | current |
| $k^2$ | figure of merit |
| $L$ | length (m) |
| $L_i$ | inductance of shunt circuit (H) |
| $L_m$ | inductance of magnetostrictive transducer (H) |
| $N$ | number of coil turns |
| $q$ | piezomagnetic coefficient |
| $R$ | resistance (Ω) |
| $R_{em}$ | transduction coefficient (m/s V) |
| $R_{me}$ | transduction coefficient (A/N) |
| $S^B$ | compliance at constant magnetic flux |
| $S^D$ | compliance at electric displacement |
| $S^E$ | compliance at constant electric field |
| $S^H$ | compliance at constant magnetic field |
| $S^I$ | compliance at constant current |
| $t$ | thickness (m) |
| $T_{em}$ | transduction coefficient (V s/m) |
| $T_{me}$ | transduction coefficient (N/A) |
| $U_e$ | electrical energy |
| $U_{em}$ | mutual energy |
| $U_m$ | elastic energy |
| $v$ | velocity |
| $V$ | voltage |
| $Y_e$ | electrical admittance |
| $Y_m$ | mechanical admittance |
| $Z_e$ | electrical impedance |
| $Z_m$ | mechanical impedance |
| $Z_{\mathrm{BC}}$ | boundary mechanical impedance |
| $\varepsilon$ | strain |
| $\mu^\sigma$ | constant stress permeability |
| $\sigma$ | stress (Pa) |
| $\phi$ | magnetic flux |
| $\xi^\sigma$ | constant stress dielectric coefficient |

conditions imposed on the component. To further complicate matters, many aerospace components experience time-varying boundary conditions. These effects are of great importance in both qualification tests and structural experimentation, such as model validation tests. When a high fidelity simulation of the system-level environments is desired, the boundary conditions during component-level testing must be well-controlled.

There are generally two approaches when accounting for component boundary conditions. With recent advances multiple-input, multiple-output (MIMO) controllers can be used to drive actuators and enforce prescribed boundary conditions. Yet on all but the simplest structures the number of degrees of freedom at the component boundaries is prohibitively large and some degrees of freedom will be necessarily be controlled passively by the impedance of the test fixturing alone. Further, complete measurements of the field motions at test control points are quite rare. Active control would require some knowledge of these motions. It may be more practical in some cases to replicate the impedances acting at the component boundaries and enforce the test specification using a traditional, single-exciter configuration. It is exactly how the uncontrolled degrees of freedom are treated that is the primary motivation of this work.

In some cases passive simulation of the component's boundary conditions may be achieved by using a section of the next-assembly as the test fixture. This was essentially the approach of Scharton [2]. Scharton's method involved using a test fixture that matched the desired boundary conditions in average sense. The average impedance was defined by using equivalent infinite plate impedance, modal density and peak-to-valley ratio. The results using these 'multimodal' test fixtures showed promise by reducing over-test as well as the input force required to conduct the test.

Use of flexible test fixtures, such as those described by Scharton [2], has recently been explored and implemented at Sandia for certain sensitive components. These fixtures generally copy the geometry of the next-assembly over a characteristic length. This approach is limited in utility for several reasons. These fixtures can be quite expensive to machine and with evolving designs may be outdated before the test can be

conducted. Also, traditional test fixtures with fixed geometry cannot take into account the stochastic nature of component boundary conditions. Further, they cannot address time-varying boundary conditions. A test fixture whose impedance could be tailored to match desired impedance functions and whose impedance could be easily adjusted would have enormous advantages over ordinary test fixtures.

In a similar scenario, where the ability to replicate a desired mechanical impedance would be of great use, a shock or vibration test machine must be calibrated prior to testing a component, but the component is unavailable for use in the calibration tests. This occurs frequently for high-value test items. In this case, it is desired to replicate the impedance of the component with a surrogate device so that the test setup may be validated prior to exposure of the high-value test article.

The goal of this work is twofold. First, it aims to enhance component-level test fidelity by improving the match between the impedance of the test fixture and that of the component's next-assembly at the degrees of freedom not controlled by the vibration test exciter. Second, it provides a means for simulating component impedance for the purposes of test setup calibration and validation. As this work demonstrates passively shunted, electromechanical transducers show promise for both these applications.

The use of shunted piezoelectric devices has been extensively explored for vibration attenuation [3–7]. The essence of these efforts is to convert mechanical energy to electrical energy using the piezoelectric material and then dissipate this energy through resistive elements. Resonant shunt circuits are designed to maximize the dissipated power in the desired frequency bands. Similar to piezoelectric materials, the mechanical properties of magnetostrictive materials are a function of magnetic boundary conditions. Magnetostrictive materials have been predominately explored for use in actuator applications [8,9] and less extensively for sensor applications [10]. Very few researchers have investigated the use of passively shunted magnetostrictive transducers for damping applications [11].

If instead of targeting dissipation of vibrational energy we design resonant shunt circuits to achieve the desired stiffness and inertia as functions of frequency we can use electromechanical transducers to mimic desired mechanical impedance functions. The work by Davis et al. [12] demonstrated the use of capacitively shunted piezoelectric devices for vibration suppression through use of a resonant absorber configuration. No previous study could be found that examined the use of electromechanical transducers for simulation of mechanical impedance functions in test fixture or test calibration applications.

Shunted electromechanical transducers can be constructed to have multiple resonances within the range of most aerospace vibration tests. These resonances can be adjusted and tuned by adjusting the v alues of the shunting electrical components, often with the twist of a knob. This allows the replication of complex, multi-modal impedance functions that can be adjusted to accommodate evolving designs or time-varying boundary conditions. Further, the cost of constructing such devices can be far less than traditional high-fidelity mock-ups of either components or their boundary constraints. These qualities make shunted electromechanical transducers an attractive opportunity for developing advanced dynamic test fixturing.

This paper develops the concepts necessary for constructing shunted electromechanical transducers that can be used to tailor the boundary impedances of high-fidelity vibration test fixtures for use in dynamic test calibration. The equations governing the mechanical impedances of such devices are derived by starting with the constitutive equations for piezoelectric and magnetostrictive materials. Concept validation is achieved through the modeling, construction and testing of such devices.

## 2. The electromechanical transducer model

By definition, transducers convert energy from one form to another. Electromechanical transducers convert electrical energy to mechanical and vice versa. The electrical and mechanical properties of the transducer vary with the mechanical and electrical boundary conditions. For instance, the magnetic permeability of magnetostrictive materials is known to vary with mechanical boundary conditions. In general, both a blocked permeability (the permeability observed when the transducer is prohibited from straining) and a free permeability (the permeability under zero load) are defined. By extension, it is not difficult to imagine that the permeability also varies with frequency as both strain and force vary with resonant mechanical boundary conditions. The goal of this work is to develop a transducer model that accounts for these electromechanical

interactions. Regardless of the specific construction or physical materials employed, Hunt [13] gives the canonical form the governing equations of an electromechanical transducer as

$$\begin{Bmatrix} V \\ F \end{Bmatrix} = \begin{bmatrix} Z_e & T_{em} \\ T_{me} & Z_m \end{bmatrix} \begin{Bmatrix} I \\ v \end{Bmatrix} \tag{1}$$

where $V$ is the voltage across the electrical terminals of the transducer, $F$ is the force developed across its mechanical terminals, $I$ is the current flowing through the electrical terminals, $v$ is the relative velocity across the mechanical terminals, $Z_e$ is the blocked (zero motion) electrical impedance, $Z_m$ is the open circuit (zero current) mechanical impedance, $T_{em}$ is a transduction coefficient whose units are volts per meter per second, and $T_{me}$ is a transduction coefficient whose units are Newtons per amp.

Hunt's canonical form, which is given in terms of impedance parameters, can be rearranged to express the behavior of the transducer in admittance quantities:

$$\begin{Bmatrix} I \\ v \end{Bmatrix} = \begin{bmatrix} Y_e & R_{em} \\ R_{me} & Y_m \end{bmatrix} \begin{Bmatrix} V \\ F \end{Bmatrix} \tag{2}$$

where $Y_e$ is the free (zero force) electrical admittance, $Y_m$ is the short circuit (zero voltage) mechanical admittance, $R_{em}$ is a transduction coefficient whose units are amps per Newton and $R_{me}$ is a transduction coefficient whose units are meters per second per volt.

The coupling coefficient, which relates the ratio of mechanical energy stored in the transducer to stored electrical energy is an important figure of merit. Following the form of Berlincourt [14], the ratio of mutual energy to the geometric mean of elastic and electrical energies is given by

$$k^2 = \frac{U_{em}^2}{U_e U_m} \tag{3}$$

Using the impedance and admittance forms of the transduction equations the electromechanical coupling coefficient for electromechanical transducers can then be expressed as

$$k^2 = \frac{R_{me} T_{em}}{Y_m Z_m^I} \tag{4}$$

where $Z_m^I$ is the mechanical impedance $F/v$ found from the condition of zero current as

$$Z_m^I = \frac{A}{sLS^I}$$

### 2.1. Piezoelectric transducers

It is assumed that vector quantities act along the direction of maximum piezoelectric activity. Following the form of Hunt [13], the basic constitutive equations governing the linear behavior of piezoelectric materials in one-dimensional, axial excitation and polarity are

$$\begin{aligned} \varepsilon &= S^E \sigma + dE \\ D &= d^X \sigma + \xi^\sigma E \end{aligned} \tag{5}$$

The superscript $(\cdot)^\sigma$ denotes constant mechanical stress, and the superscript $(\cdot)^E$ denotes measurements taken at constant electric field. If the transduction process is completely reversible then $d^X = d$.

From the definition of electric displacement,

$$D = \frac{Q}{A} = \frac{1}{A} \int I \, \mathrm{d}t \tag{6}$$

the definition of electric field,

$$E = \frac{V}{t} \tag{7}$$

and introducing the Laplace variable, $s = j\omega$, the canonical impedance form for piezoelectric transducers in the linear regime is found to be given by

$$\begin{Bmatrix} V \\ F \end{Bmatrix} = \begin{bmatrix} \dfrac{t}{As\xi^{\sigma}(1-k^2)} & \dfrac{-d}{S^E s\xi^{\sigma}(1-k^2)} \\ \dfrac{-d}{S^E s\xi^{\sigma}(1-k^2)} & \dfrac{A}{tsS^E(1-k^2)} \end{bmatrix} \begin{Bmatrix} I \\ v \end{Bmatrix} \tag{8}$$

The electromechanical coupling coefficient for piezoelectric materials can then be found as $k^2 = d^2/S^E\xi^{\sigma}$. Typical values of the coupling coefficient for PZT range from 0.3 to 0.69. In the open-circuit case $\varepsilon = S^D\sigma$, where $(\cdot)^D$ denotes measurements taken at constant electric displacement, while for the short-circuit case $\varepsilon = S^E\sigma$. The two compliances are related by the expression $S_D = S^E_{3,3}(1-k^2_{3,3})$.

The canonical admittance form, which we will find to be slightly more practical than the impedance form, is given by

$$\begin{Bmatrix} I \\ v \end{Bmatrix} = \begin{bmatrix} \dfrac{As\xi^{\sigma}}{t} & ds \\ ds & \dfrac{S^E st}{A} \end{bmatrix} \begin{Bmatrix} V \\ F \end{Bmatrix} \tag{9}$$

Note that Eqs. (8) and (9) describe the behavior of a transducer consisting of a single, monolithic element of piezoelectric material. However, many useful piezoelectric transducers are composed of layers of piezoelectric material bonded together. A mechanical preload can also be added to both enhance the piezoelectric properties [15–17] and to prevent the material from experiencing tensile stresses under which it may be fragile. The piezoelectric material parameters short circuit compliance $S^E$, permittivity $\xi$, and the piezoelectric coupling coefficient $d$, all appear in the expression for the electromechanical transducer model. Because of the dependence of all of these parameters with preload [15–17], the best transducer model can be had by direct measurement of the admittance parameters in Eq. (2).

If direct measurements cannot be made, theoretical considerations can provide insight into incorporating some of the practical aspects of piezoelectric transducer construction as follows. The mechanical admittances of the stiffness of individual layers of material in series add directly, as do the electrical admittances of the individual capacitances in parallel. The transduction coefficient $R_{em} = R_{me}$ is dependent on the piezoelectric charge constant, $d$. The piezoelectric charge constant relates the charge produced in response to a mechanical stress. With the assumption of constant force throughout the transducer (dynamic effects in the transducer are ignored) the charges produced by each layer connected in electrical parallel also add directly. The concept validation section demonstrates how the transducer parameters can be adjusted through a combination of direct measurement and theoretical considerations.

### 2.2. Magnetostrictive transducers

Magnetostrictive materials strain due to an applied magnetic field, or generate a magnetic flux density due to an applied stress. Magnetostriction results from the rotation of magnetic domains aligning with an applied magnetic field. The cumulative effect of the sum of these aligned rotations is the observed positive strain of the material. Because domain alignment in either the $0^\circ$ or $180^\circ$ directions brings about the same strain, magnetostrictive transducers are operated around a static magnetic field bias so that linear operation is achieved under AC drive conditions [18].

It is assumed that vector quantities are directed along the direction of maximum response and activity. Following the form of Ref. [18], the linear, small-signal, constitutive equations governing magnetostrictive transduction are

$$\begin{aligned} \varepsilon &= S^H\sigma + qH \\ B &= q^X\sigma + \mu^{\sigma}H \end{aligned} \tag{10}$$

where the superscript $(\cdot)^H$ denotes constant magnetic field intensity (usually accomplished through an open circuit) the superscript $(\cdot)^\sigma$ denotes constant mechanical stress (usually achieved through a free, unloaded transducer).

If the transduction process is completely reversible, $q^X = q$. Magnetic field intensity is given by

$$H = \frac{N}{L} I \tag{11}$$

where $N$ is the number of turns in the coil around the length of the core $L$, and $I$ is the current flowing in the coil. Faraday's law states that $V = -N(\mathrm{d}\phi/\mathrm{d}t)$ where $\phi$ is the magnetic flux. With $\phi = BA$ and again introducing the Laplace variable, $s = j\omega$ we have $B = -V/NAs$. After substitution into Eq. (10), the canonical impedance form for linear magnetostrictive transducers is found to be given by

$$\begin{Bmatrix} V \\ F \end{Bmatrix} = \begin{bmatrix} \dfrac{N^2 A s \mu^\sigma (1-k^2)}{L} & \dfrac{qAN}{S^H L} \\ \dfrac{-qAN}{S^H L} & \dfrac{A}{S^H L s} \end{bmatrix} \begin{Bmatrix} I \\ v \end{Bmatrix} \tag{12}$$

The electromechanical coupling coefficient for magnetostrictive materials can then be found as $k^2 = q^2/S^H\mu^\sigma$. Typical values of $k^2$ for magnetostrictive Terfenol-D range from 0.7 to 0.75.

For the open-circuit case $\varepsilon = S^H\sigma$ while for the short-circuit case $\varepsilon = S^B\sigma$, where $(\cdot)^B$ denotes constant flux intensity (usually achieved through a short circuit). The compliances are related such that $S^B = S^H(1-k^2)$.

The canonical admittance form can then be found as given by Eq. (15).

$$\begin{Bmatrix} I \\ v \end{Bmatrix} = \begin{bmatrix} \dfrac{L}{sN^2 A\mu^\sigma} & -\dfrac{qL}{\mu^\sigma NA} \\ \dfrac{qL}{\mu^\sigma NA} & \dfrac{sLS^H(1-k^2)}{A} \end{bmatrix} \begin{Bmatrix} V \\ F \end{Bmatrix} \tag{13}$$

In contrast to the stacked construction of most piezoelectric actuators, magnetostrictive transducers are usually constructed of a single, monolithic magnetostrictive core. Similar to PZT, an increase in the magnetostrictive coupling of Terfenol-D can be had with preload [18,19]. The preload is also desirable to prevent the Terfenol-D core from experiencing tensile loads due to fragility in tension [18]. An additional bias in the induced magnetic field $H$ is also desirable to linearize the strain versus field behavior [18]. The magnetostrictive parameters permeability, $\mu^\sigma$, compliance $S^H$, and coupling coefficient $q$ all appear in the electromechanical transducer model. Because all these parameters vary with preload and magnetic bias [19,20], the most accurate transducer model can be had through direct measurement of the parameters in Eq. (2).

The impedance and admittance parameters for both transducer types are summarized in Tables 1 and 2.

Table 1
Transducer impedance parameters.

| Impedance parameters | Piezoelectric transducers | Magnetostrictive transducers |
|---|---|---|
| $Z_m$ | $\dfrac{A}{tsS^E(1-k^2)}$ | $\dfrac{A}{S^H L s}$ |
| $Z_e$ | $\dfrac{t}{As\xi^\sigma(1-k^2)}$ | $\dfrac{N^2 A s\mu^\sigma(1-k^2)}{L}$ |
| $T_{em}$, $T_{me}$ | $T_{em} = T_{me} = \dfrac{-d}{S^E s\xi^\sigma(1-k^2)}$ | $T_{em} = -T_{me} = \dfrac{qAN}{S^H L}$ |

Table 2
Transducer admittance parameters.

| Admittance parameters | Piezoelectric transducers | Magnetostrictive transducers |
|---|---|---|
| $Y_m$ | $\frac{S^E st}{A}$ | $\frac{sLS^H(1-k^2)}{A}$ |
| $Y_e$ | $\frac{As\xi^\sigma}{t}$ | $\frac{L}{sN^2A\mu^\sigma}$ |
| $R_{em}$, $R_{me}$ | $R_{em}=R_{me}=ds$ | $R_{em}=-R_{me}=\frac{qL}{\mu^\sigma NA}$ |

Table 3
Shunted transducer parameters.

| Shunted parameters | Piezoelectric transducers | Magnetostrictive transducers |
|---|---|---|
| $\tilde{Z}_m$ | $Z_m\frac{1+\frac{Y_{\rm sh}}{Y_e}}{\left[1+\frac{Y_{\rm sh}}{Y_e(1-k^2)}\right]}$ | $Z_m\frac{1+\frac{Y_{\rm sh}}{Y_e}}{\left[1+\frac{Y_{\rm sh}(1-k^2)}{Y_e}\right]}$ |
| $\tilde{Z}_e$ | $Z_e\frac{1}{1+Y_{\rm sh}Z_e}$ | $Z_e\frac{1}{1+Y_{\rm sh}Z_e}$ |
| $\tilde{T}_{em}$, $\tilde{T}_{me}$ | $\tilde{T}_{em}=\tilde{T}_{me}=T_{em}\frac{1}{\left[1+\frac{Y_{\rm sh}}{Y_e(1-k^2)}\right]}$ | $\tilde{T}_{em}=-\tilde{T}_{me}=T_{em}\frac{1}{\left[1+\frac{Y_{\rm sh}(1-k^2)}{Y_e}\right]}$ |

### 2.3. The electrical shunt

In this work, we are interested in taking advantage of the coupled nature of the electrical and mechanical impedances of electromechanical transducers. We desire to induce a specific mechanical impedance by tailoring the transducer's electrical boundary conditions. This will be accomplished through the use of a passive, parallel, resonant shunt circuit. The effects of the electrical shunt are added directly to the electrical admittance of the transducer as

$$\begin{Bmatrix} I \\ v \end{Bmatrix} = \begin{bmatrix} Y_e + Y_{\rm sh} & R_{em} \\ R_{me} & Y_m \end{bmatrix} \begin{Bmatrix} V \\ F \end{Bmatrix} \tag{14}$$

Eq. (14) can be inverted to solve for the transducer impedance parameters when the electrical shunt is added. The results for both piezoelectric and magnetostrictive transducers are shown in Table 3.

From the expressions for the shunted mechanical impedance it is clear that when $Y_{\rm sh}/Y_e \to -1$ the shunted mechanical impedance goes to zero $\tilde{Z}_m \to 0$, indicating mechanical resonances. Since in both the piezoelectric and magnetostrictive cases the ideal electrical admittance is purely reactive, the goal of shunt circuit design is to ensure that $-\mathrm{Im}(Y_{\rm sh}) = Y_e$ at the desired frequencies. The mechanical boundary conditions will also affect the resonance frequencies of the shunted transducer, and must be accounted-for as described in the following section.

Although different approaches have been developed [6,21,22], the so-called current-flowing [22] approach to multi-mode shunt circuit design is quite practical and was used in the design of shunt circuits for this work.

### 2.4. Predicting shunted transducer mechanical impedance

In most real-world scenarios, the electromechanical transducer has two mechanical terminals, one at each end of the transducer. The tacit assumption in Eq. (2) is that one of the mechanical terminals is grounded. With one terminal grounded, driving point resonances occur where $\tilde{Z}_m + Z_{\mathrm{BC1}} \to 0$ where $Z_{\mathrm{BC1}}$ is the impedance of the attached load. When the load is a is a non-resonant mass, $Z_{\mathrm{BC1}}$ is purely imaginary and loaded-transducer resonances occur where $\mathrm{Re}(\tilde{Z}_m) \to 0$ and $-\mathrm{Im}(\tilde{Z}_m) = Z_{\mathrm{BC1}}$. A typical case is depicted in Fig. 1. The condition $-\mathrm{Im}(Y_{\mathrm{sh}}) = Y_e$ is satisfied at 850 Hz so the unloaded resonance occurs at this frequency. The mechanical boundary condition drives the first resonance to 588 Hz and induces the second resonance at 1036 Hz.

True mechanical ground is much more difficult to achieve than electrical ground. In most cases both the mechanical boundary conditions must be taken into account to accurately predict the performance of the system. A degree of freedom must be added to the equations to account for the second mechanical terminal as

$$\begin{Bmatrix} V \\ F_1 \\ F_2 \end{Bmatrix} = \begin{bmatrix} Z_e & T_{em} & -T_{em} \\ T_{me} & Z_m + Z_{\mathrm{BC1}} & -Z_m \\ -T_{me} & -Z_m & Z_m + Z_{\mathrm{BC2}} \end{bmatrix} \begin{Bmatrix} I \\ v_1 \\ v_2 \end{Bmatrix} \tag{15}$$

where $Z_{\mathrm{BC1}}$ and $Z_{\mathrm{BC2}}$ are the mechanical boundary conditions of the transducer.

Before the mechanical impedance of the shunted transducer is known, Eq. (1), or equivalently Eq. (3), are underdetermined as either the current or voltage must be known to solve the equations for total mechanical impedance, $F/v$. From the second line of Eq. (15), with shunted parameters from Table 3, it can be seen that the total driving point mechanical impedance as would be measured experimentally is

$$\frac{F_1}{v_1} = \frac{\tilde{T}_{me} I}{v_1} + [\tilde{Z}_m + Z_{\mathrm{BC1}}] - \tilde{Z}_m \frac{v_2}{v_1} \tag{16}$$

while the total transfer mechanical impedance is

$$\frac{F_1}{v_2} = \frac{\tilde{T}_{me} I}{v_2} + [\tilde{Z}_m + Z_{\mathrm{BC1}}] \frac{v_1}{v_2} - \tilde{Z}_m \tag{17}$$

In order to obtain predictions for mechanical impedance assumptions must be made to reduce the number of unknowns.

One reasonable approach is to assume that no current flows across the transducer, that is $I = 0$. Under this open-circuit assumption, the mechanical impedance of the shunted transducer can be estimated from Eq. (14) as

$$\tilde{Z}_m \cong \frac{F}{v_{I=0}} = \left[ Y_m - \frac{R_{em} R_{me}}{Y_e + Y_{\mathrm{sh}}} \right]^{-1} \tag{18}$$

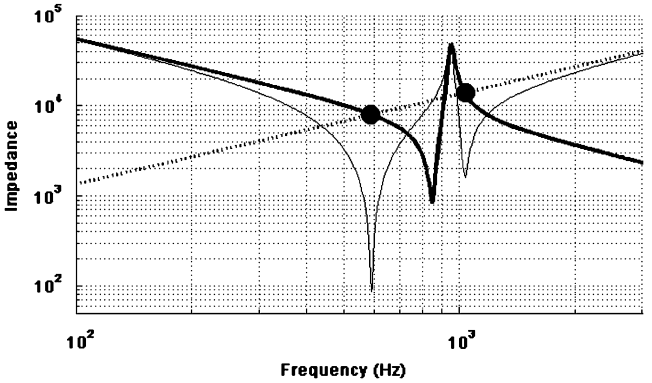


Fig. 1. Fixed-base, loaded transducer resonances: ———, $\tilde{Z}_m$; ▪▪▪▪▪▪, $Z_{\mathrm{BC1}}$; ● – $\mathrm{Im}(Z_m) = Z_{\mathrm{BC1}}$; and ———, fixed-base, loaded impedance.

This approach provides a useful approximation for predicting the total mechanical impedance for design purposes.

## 3. Implementation

In general, aerospace vibration tests are conducted in the range of 20 Hz to 5 kHz. Therefore, any useful variable impedance test fixtures will be able to approximate resonant impedance functions within this range. The mechanical impedance of both transducers is a function of the uncoupled mechanical compliance. The term 'uncoupled' is used to describe the case in which the electromagnetic storage mechanisms are prevented from participating. For magnetostrictive transducers the uncoupled compliance is the open-circuit compliance while for piezoelectric transducers the short-circuit compliance is uncoupled. In order for shunt circuit elements to have a useful effect on the mechanical impedance of the transducer, the uncoupled resonance of the loaded transducer must be near the desired shunted resonant frequencies. Otherwise, the impedance of the transducer is large and the electrical shunt has little effect on the mechanical impedance.

Bringing the uncoupled resonance of the transducer in the desired range can be a challenging task. PZT ceramics are quite stiff and light, making the first open-circuit resonance of these unloaded transducers in the range of 3–10 kHz. Conversely, the constant field compliance of Terfenol-D is approximately twenty times the constant field compliance of PI-151 [18] making Terfenol-D transducers an attractive choice for this application. Geometrical considerations involving mechanical advantage can be used to lower the effective stiffness of both transducer types.

Piezoelectric polymers, such as PVDF, are much more compliant (on the order of 10–20 times more compliant) than either soft PZT or Terfenol-D [23] but the coupling factor $k^2$ of piezoelectric polymers is much lower than those of piezoelectric ceramic materials (0.01 versus 0.5) [23]. Because the coupling factor represents the ability of the transducing material to convert mechanical energy to electrical energy a low coupling factor limits the ability of the shunt circuit to adjust the mechanical impedance of the device. As can be seen from the expressions in Table 3 for piezoelectric transducers, lowered values of $k^2$ tend to decrease the effective electrical admittance of the transducer compared to higher values of $k^2$, making the transducer less receptive to modification by $Y_{\mathrm{sh}}$. It is clear from these expressions that as $k^2 \to 0$ then $\tilde{Z}_m \to Z_m$. Generally, their low coupling factor precludes the use of piezoelectric polymer transducers in these applications.

Examination of the expressions shown in Table 3 for $\tilde{Z}_m$ reveals an important difference between the two transducer types. The expressions are of the same form; however, the ratio of electrical shunt admittance to electrical transducer admittance that appears in both expression is quite different between the two transducer types. The higher electrical admittance (low impedance) of magnetostrictive transducers at low frequencies makes them more receptive to low-frequency electrical resonances of the electrical shunt circuit than the low electrical admittance (high impedance) of piezoelectric transducers. This makes passively shunted magnetostrictive transducers better able to replicate lightly damped mechanical resonances in lower frequencies than piezoelectric transducers. The concept is equivalent to impedance matching in power transmission systems.

Of very practical importance is the electrical output expected from the electromechanical transducers. The magnitude of the electrical output is an important consideration for both safety and design of the shunt circuitry, which may require high-voltage or high-current considerations. Before the addition of the shunt circuit, the transduction coefficient $T_{em}$, whose units are volts per meter per second, indicate that the sensitivity of piezoelectric transducers is an inverse function of frequency and independent of the area of the sensing material. The transduction coefficient of magnetostrictive transducers is independent of frequency, but depends on transducer area. Substituting nominal constitutive parameters for PI 151 and Terfenol-D transducers into these expressions reveals that the transduction coefficient of piezoelectric transducers can be several orders of magnitude higher than that of magnetostrictive transducers over the frequency range of interest.

When the passive shunts are added in parallel to the transducers, the transduction coefficients of both transducer types become resonant functions of frequency. For piezoelectric transducers $T_{em}$ is a decreasing function of frequency so that away from electrical resonance $\tilde{T}_{em}$ will be large at low frequencies and low at high frequencies. The appearance of $1 + Y_{\mathrm{sh}}/Y_e(1-k^2)$ in the denominator indicates that $\tilde{T}_{em}$ is maximized

where $Y_{sh}/Y_e = -(1-k^2)$. The ideal electrical admittance is purely reactive and positive for piezoelectric transducers. In general, the electrical admittance of the shunt is both resistive and reactive, with the reactive part being positive for frequencies less than electrical resonance and negative for frequencies greater than resonance. This indicates $\tilde{T}_{em}$ for piezoelectric transducers reaches a minimum near the shunt resonance and a maximum above the resonant frequency of the shunt.

For magnetostrictive transducers $T_{em}$ is not a function of frequency so that away from electrical resonance $\tilde{T}_{em}$ is constant. Near electrical resonance $\tilde{T}_{em}$ is maximized where $Y_{sh}/Y_e = -1/(1-k^2)$. The ideal electrical admittance of magnetostrictive transducers is purely reactive and negative. This indicates that $\tilde{T}_{em}$ for magnetostrictive transducers reaches a maximum below the resonance of the shunt and a minimum near the resonance of the shunt.

The effects of the electrical admittances of the transducer and shunt described above may cause the electrical output of magnetostrictive transducers to exceed that of piezoelectric transducers at some frequencies, as can be seen in Fig. 2. A careful analysis of expected electrical outputs for a given test setup is warranted, as this has implications for both safety and the design of the shunt circuits, which may require high-voltage components. The voltage output of some passively shunted transducer designs in dynamic test fixture applications may exceed hundreds of volts per unit acceleration across the two mechanical ports of the transducer.

Finally, practical aspects of incorporating these transducers into dynamic test fixtures must considered. Both piezoelectric and magnetostrictive materials are fragile under tension. Both transducer types usually incorporate preloading mechanisms to prevent the sensing material from coming under tension. However, both transducer types must be protected from bending loads. Frequently, double-hinged connections are used to isolate the transducer from bending.

### 3.1. Nonlinear behavior

The transduction equations assume the transducer is both linear and conservative. Although these approximations are useful and frequently made, they are not accurate for PZT or Terfenol-D in so-called large signal regimes. Large values of either mechanical or electrical stimulus can drive both PZT and Terfenol-D transducers into a nonlinear state. When used in vibration test fixtures these transducers may be exposed to large signals as both mechanical and electrical resonances will be encountered. Therefore, nonlinear effects must be considered. Unfortunately, most researchers have studied the nonlinearities of driven actuators [8,24–26,28]. Several have focused on the effects of hysteresis in active damping applications [27,36]. Few, if any, have studied the effects of nonlinear behavior on the mechanical impedance of passively shunted transducers.

In general, only nonlinear behavior in the mechanical impedance is of interest. Electrical nonlinearities and variation in the constitutive parameters are only of interest insomuch as they affect the passive mechanical impedance of the shunted transducer. Nonlinear and hysteretic relations between force and displacement is of primary interest because it will limit the ability of the practitioner to achieve the desired mechanical impedance. Harmonic distortion observed between open-loop electrical drive and transducer displacement

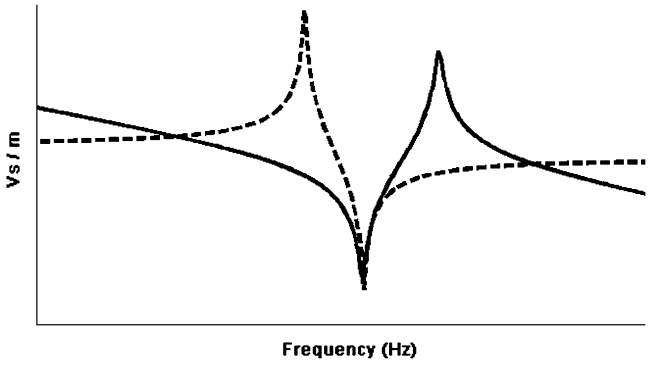


Fig. 2. Notional shunted transducer transduction coefficients: ———, piezoelectric; and – – – –, magnetostrictive.

[8,29] or with an attached, resonant payload, such as observed in Refs. [24,30] is expected due to feedback from the payload and not significant in this application.

When large loads are applied to piezoelectric ceramics the responses exhibit significant nonlinear and hysteretic response [15–17,31,32]. These nonlinearities are induced by reorientation of the polarized domains due to either electrical (ferroelectric) or mechanical (ferroelastic) loading [15,32,33]. The strain versus electric displacement, $D$, is nearly linear and anhysteretic, however [27,34,35]. Examination of the transducer equations for piezoelectric transducers reveals that force is dependent on the integral of electrical current. Since strain versus electric displacement is nearly linear and anhysteretic and since electric displacement is proportional to the integral of current through Eq. (6), it follows that force versus displacement should be near linear and anhysteretic provided that the constitutive parameters are constant. However, it is known that the mechanical compliance of piezoelectric ceramics also exhibit nonlinearity attributed to reorientation of the domains [34]. The compliance of both hard and soft PZT is shown to become markedly nonlinear over 20 MPa, with large hysteresis [32,34]. Soft PZT also shows a strong tendency for residual strain upon unloading. Further, the compliance of soft PZT is different in tension and compression [37]. These effects suggest that the constitutive parameters are far from constant.

The piezoelectric strain coefficient, $d$, depends on both frequency of alternating stress and stress magnitude [38]. It can increase by more than 100 percent with both electric field, $E$ and stress amplitude over the small-signal value, but decreases with stress frequency [34,38]. It has also been shown that the phase relation between field and stress is significant [16]. The permittivity, $\xi^{\sigma}$, is also known to vary significantly with field [34]. Both electric displacement and strain, $\varepsilon$, exhibit hysteresis versus electric field [16,32]. These effects will certainly produce harmonic distortion in the mechanical impedance of passively shunted piezoelectric transducers.

Terfenol-D also displays nonlinear and hysteretic behavior under large loads. The nonlinear effects observed in magnetostrictive materials are due to the intersection of rotating domains with material inclusions [39]. The inclusions provide pinning sites due to the reduction in energy associated with intersection of the domain wall and the inclusion. For small variations in magnetic field intensity, the magnetization of the material is reversible and anhysteretic. For large applied magnetic field the domain walls intersect remote pinning sites and the magnetization is not totally reversible. Magnetization versus applied magnetic field is hysteretic [18,39] due to the energy loss as domains transit the pinning sites [39]. The strain versus magnetic flux density curve of Terfenol-D is nearly anhysteretic and nonlinear [18,20,39], but approximately linear over a useful range. The combination of these effects results in a nonlinear and hysteretic strain versus applied magnetic field curve.

The transducer equations for magnetostrictive transducers indicate that force is directly related to electrical current instead of through differential or integral quantities as in the case of piezoelectric transducers. Since strain versus field intensity, $H$, is hysteretic for Terfenol-D and since magnetic field intensity and current are related through Eq. (11), it is anticipated that force versus displacement for passively shunted Terfenol-D transducers will also be hysteretic. This is the result shown by Moffett et al. [19] at constant field intensity. Further, the permeability, $\mu^{\sigma}$, piezomagnetic coefficient, $q$, and open-circuit compliance, $S^{H}$, of Terfenol-D are somewhat nonlinear with transducer drive [19,25,29,40,41]. But, Moffet et al. [19] show that these parameters become more linear versus drive level with favorable magnetic and stress bias. Further, they show that at reasonable bias levels, the parameters vary by approximately 25 percent with drive level. Clark et al. [20] also show that the parameters are nearly constant over a useful range of drive and vary by approximately 25 percent over the range of stress and field drive levels reported. Dapino et al. [40] show approximately the same 25 percent variation of parameter values over a range of applied field values, but also show the significant statistical variation in these estimates. It has been suggested that the linear model of magnetostriction is reasonable for strains up to one third the maximum attainable strain [40]. Still, given the hysteretic behavior of force versus displacement, even under the assumption of constant parameter values, will lead to harmonic distortion in the mechanical impedance of passively shunted magnetostrictive transducers.

Clearly, both piezoelectric and magnetostrictive transducers suffer from nonlinearities when driven past the small-signal range. It is not obvious which of these materials will behave more favorably in passively shunted transducers. Piezoelectric transducers have a near linear, anhysteretic mechanical impedance behavior under the assumption of constant parameters, but the parameters are known to vary by greater than 100 percent.

Magnetostrictive transducers have a hysteretic mechanical impedance, but the parameters are much more constant with drive level than those of PZT.

The hysteresis observed in both mechanical and the electromagnetic quantities can be compared for the two materials over their respective useful ranges. The stress versus strain hysteresis for Terfenol-D given by Moffett et al. [19] is much smaller than the stress versus strain hysteresis for the PZT in Fan et al. [32] and Fang and Li [31]. The hysteresis of strain versus electric field for soft PZT in Zhou et al. [15] and Fang and Li [31] is much larger than the comparable strain versus magnetic field for Terfenol-D given by Moffett et al. [19]. Similarly, the hysteresis in the relation of electric displacement versus electric field for PZT given in Zhou et al. [15] and Fang and Li [31] is much larger than the hysteresis between magnetic flux versus magnetic field intensity for Terfenol-D given by Calkins et al. [39]. Although the results depend on bias conditions, it appears that in all these cases, the soft PZT exhibits on the order of ten times the hysteresis of Terfenol-D.

Given the reduced hysteresis and reduced variation in parameters compared to PZT, it is believed that passively shunted Terfenol-D transducers will behave in a more linear fashion than will passively shunted transducers constructed of PZT, especially soft PZT.

## 4. Concept validation

Concept validation devices were constructed to demonstrate the use of shunted electromechanical transducers in replicating desired mechanical impedance functions in the frequency range of ordinary aerospace vibration testing. A soft PZT material manufactured by PI Ceramic, PI 151, was chosen because of its coupling factor and its high compliance compared to most PZT materials. A table of relevant PI 151 properties [42] appears in Table 4.

Non-resonant masses were attached to each of the mechanical terminals as shown in Fig. 3 to provide well-defined transducer boundary conditions and thus minimize the experimental uncertainty. The length and cross-sectional area of the transducer were chosen to bring the uncoupled resonance, including the transducer boundary conditions, into the useful frequency range. The layers of PI 151 were connected in electrical parallel to increase the capacitance of the transducer and reduce the inductance required to target mechanical resonances in the useful frequency range. The electrical shunt was added in parallel across the transducer. Table 5 gives relevant parameters of the validation device.

The transducer parameters were determined partially from experimental measurements and partially from theoretical developments. The electrical mobility of the transducer under free–free mechanical boundary conditions was measured experimentally using a Hewlett Packard 4192A impedance analyzer. Interestingly, the electrical impedance was found to have a real component that varies as $\frac{1}{f}$. The mechanical impedance was first estimated using theoretical considerations and then refined through the modeling the additional impedance of a compensating spring in series with the actuator. The physical interpretation of such a spring is to account for the effects such as the adhesive used to bond the layers of piezoceramic that increase the uncoupled compliance of the transducer. The compliance of the compensating spring is found from the short circuit resonance frequency of the transducer because, as can be seen in Eq. (2), the transduction coefficient $R_{em}$ is not effective under short circuit conditions. The open-circuit mechanical impedance was then estimated using Eq. (18), substituted into Eq. (15) with $I = 0$, and compared to the experimental measurements. Because most experimental data is measured in terms of acceleration the predicted impedance was converted to

Table 4
Relevant properties of PI 151.

| Parameter | Value |
|---|---|
| Permittivity: $\varepsilon_{33}^T/\varepsilon_0$ | 2400 |
| Coupling factor: $k_{33}$ | 0.69 |
| Charge constant: $d_{33}$ | $500 \times 10^{-12}$ C/N |
| Voltage constant: $g_{33}$ | $22 \times 10^{-3}$ V m/N |
| Elastic compliance: $S_{33}^E$ | $19 \times 10^{-12}$ m$^2$/N |

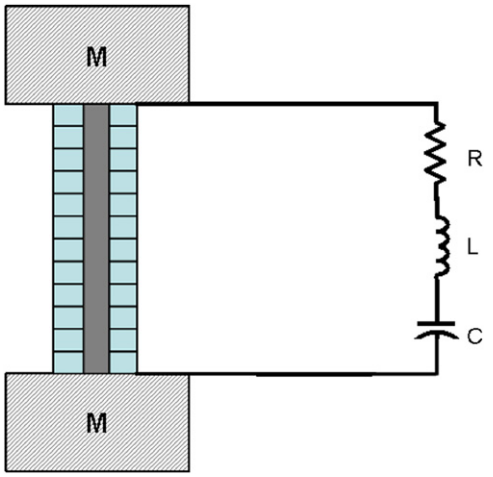


Fig. 3. Concept validation device.

Table 5
Validation device parameters.

| Parameter | Value |
|---|---|
| $M$ (kg) | 1.75 |
| Length (mm) | 104 |
| Cross-sectional area ($m^2$) | $5.89 \times 10^{-5}$ |
| Internal capacitance (F) | $360 \times 10^{-9}$ |

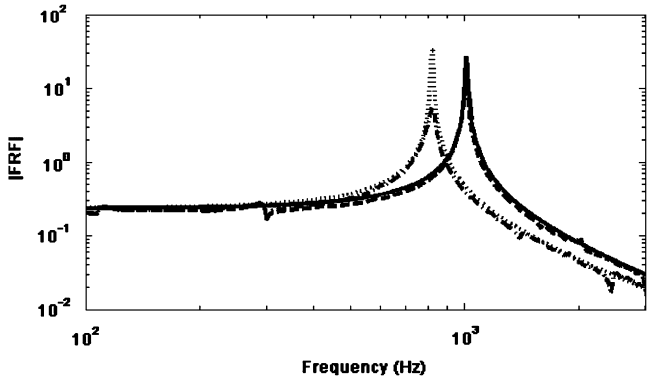


Fig. 4. Open and short-circuit results: ———, open circuit, predicted; – – – –, open circuit, measured; ▪▪▪▪▪▪, short circuit, predicted; and — ▪ — ▪, short circuit, measured.

accelerance using the relation $\boldsymbol{A} = s\mathbf{Z}^{-1}$. The short-circuit data used in this procedure can be seen in Fig. 4. With the value of the compensating spring determined, the open-circuit admittance is then used to adjust the value of the transduction coefficient $R_{me} = R_{em}$. This completes the characterization of the un-shunted transducer.

Two single-resonant shunt circuits were modeled, constructed and placed across the transducer to achieve the desired mechanical impedance functions. In the first configuration the shunt parameters were $L = 0.5H$, $C = 0.33\mu F$ and $R = 20\,\Omega$. The second configuration utilized shunt parameters $L = 0.2H$, $C = 0.33\mu F$ and $R = 10\,\Omega$. The open-circuit mechanical impedance was then estimated using Eq. (18). The predicted and

measured transfer accelerance functions can be seen in Figs. 5 and 7, respectively. The effects of some transverse modes, which are not accounted for in the model, can be seen in the lower frequencies.

A nonlinear trend is evident in both shunted results. The frequency of the higher resonance is slightly underestimated in Configuration #1, and further underestimated in Configuration #2. Damjanovic [38] observed that the piezoelectric coefficient $d$ increases with increasing alternating stress. It is postulated that the underestimation of stiffness in the second mode is due to a change in $d$ resulting from the increased stress at that frequency. Damjanovic also observed a decrease of $d$ with increasing stress frequency, but this dependence is about 4 percent per decade while the increase in $d$ with increasing stress is about 30 percent per decade.

Stress per unit input force in the transducer was estimated from the three experimental measurements and appears in Fig. 11. Stress at the second resonance is 225 percent higher in Configuration #1 and 525 percent higher in Configuration #2 compared to the open-circuit case, from which the value of $R_{em}$ was initially determined. As the first and second mode are closer together in frequency the stress at the second resonance is higher due to superposition, which tends to raise the piezoelectric coefficient at that frequency. The maximum stress over all frequencies occurs in Configuration #1, but this maximum stress occurs at the frequency of the electrical anti-resonance. The piezoelectric coefficient appears to be most sensitive to the stress at the mechanical resonance.

Note from Table 3 that $\tilde{Z}_m$ is not dependent on piezoelectric charge constant, $d$, while the total observed mechanical impedance, $F/v$, is dependent on $d$ through the appearance of $T_{em}$ in Eqs. (16) and (17). While they are not uncoupled, in this case the first resonance is most closely associated with the condition of $-\mathrm{Im}(Y_{\mathrm{sh}}) = Y_e$ in the unloaded transducer while the second is most closely associated with the mechanical resonance induced by the load at the frequency where $-\mathrm{Im}(\tilde{Z}_m) = Z_{\mathrm{BC}}$. Because neither $Y_{\mathrm{sh}}$ nor $Y_e$ depend on $d$, the frequency of the first resonance is not strongly dependent on $d$.

In an apparent confirmation of the source of the increased stiffness observed in the second resonance frequency, the change in piezoelectric coefficient with stress, the transduction coefficient $R_{em} = R_{me}$ used to estimate $\tilde{Z}_m$ using $F/v_{I=0}$ by Eq. (18), was increased by 12 percent and the Configuration #2 analysis was performed with this adjusted value. This is approximately the increase in $d$ reported by Damjanovic [38] for a 500 percent increase in alternating stress amplitude. The results appear in Fig. 9. Although deviations between predicted and measured responses are evident, the natural frequencies are accurately predicted. The additional deviations may be due the neglect of the electrical feedback and nonlinear or hysteretic effects. The shape of the imaginary part of the experimental data as plotted in Fig. 10 suggests some mild nonlinearity as it is not entirely symmetric about the resonance frequencies.

Once the mechanical impedance is estimated using the open-circuit assumption, the validity of the assumption can be tested by substituting the estimated mechanical impedance into Eq. (15) and solving for current using the measured velocities. From Eq. (16) the current can be found as

$$I = \frac{1}{\tilde{T}_{me}}[1 - [\tilde{Z}_m + Z_{\mathrm{BC1}}]v_1 + \tilde{Z}_m v_2] \tag{19}$$

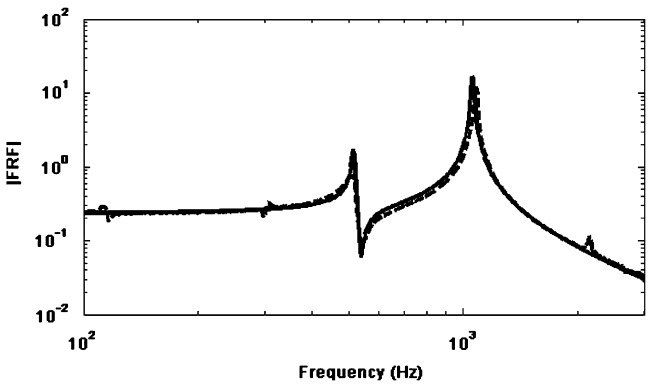


Fig. 5. Configuration #1 results: ———, predicted; and – – – –, measured.

while the voltage can be found from the first line of Eq. (3) as

$$V = I\tilde{Z}_e + \tilde{T}_{em}[v_1 - v_2] \tag{20}$$

In both of the above equations, the appropriate measured mechanical mobility was substituted for velocities to find current and voltage per unit input force. The results can be seen in Figs. 6 and 8. It appears that the assumption of zero current is reasonable as the maximum estimated current was less than 20 mA.

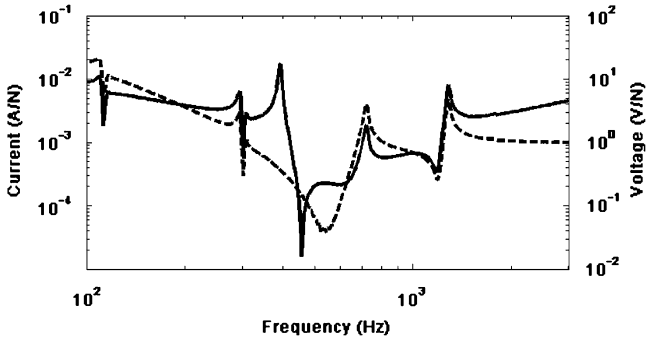


Fig. 6. Estimated current and voltage, configuration #: ———, current; and – – – –, voltage.

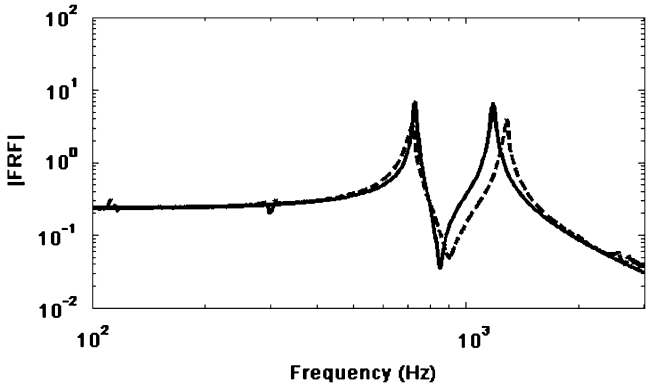


Fig. 7. Configuration #2 results: ———, predicted; and – – – –, measured.

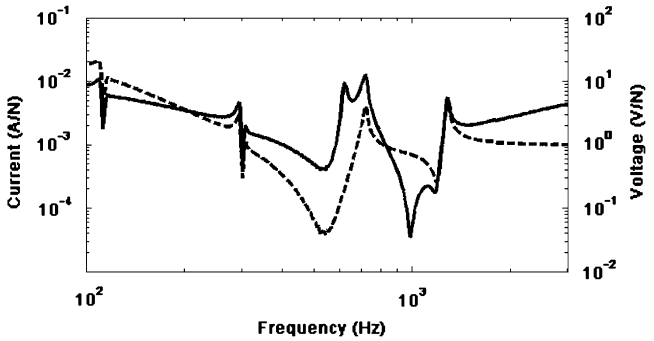


Fig. 8. Estimated current and voltage, configuration #2: ———, current; and – – – –, voltage.

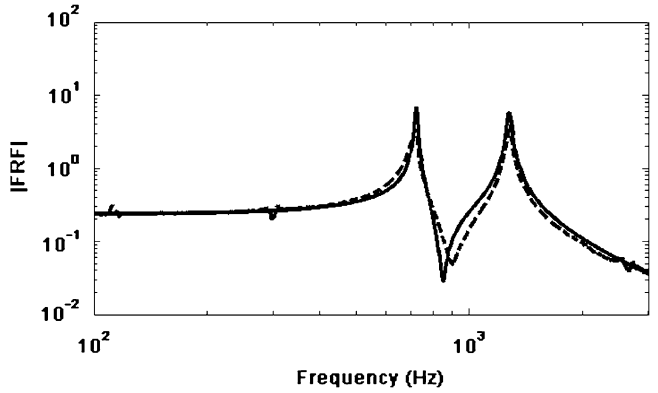


Fig. 9. Configuration #2 results, $R_{em}$ adjusted: ———, predicted; and – – – –, measured.

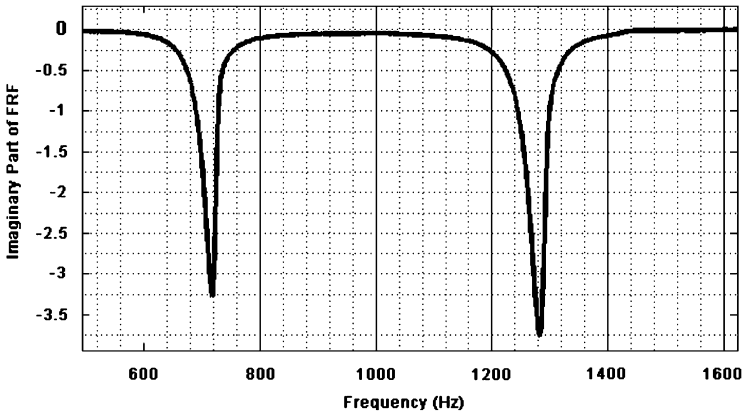


Fig. 10. Imaginary part of FRF showing slight nonlinearities for configuration #2.

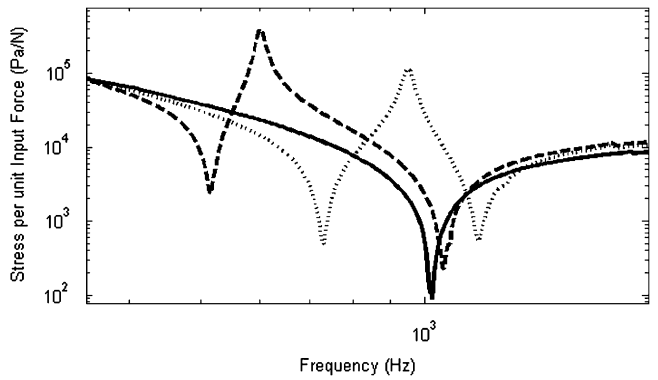


Fig. 11. Estimated stress per unit input force: open and short-circuit results: ———, open circuit; – – – –, configuration #1; and ▪▪▪▪▪▪, configuration #2.

## 5. Conclusions

The need to accurately simulate component boundary conditions is great. Instances of component failure in component-level shock and vibration tests have occurred due to unrealistic boundary conditions. It is almost

certain that others have inappropriately passed dynamic testing because of the same effects. In some cases, multiple actuators and a MIMO controller can be used to actively enforce boundary conditions at component degrees of freedom. Even when such technology is available it is seldom practical to actively control every boundary degree of freedom and some will be controlled by the test fixture out of necessity.

Fixtures that replicate a characteristic length of the geometry of the next assembly can be used to improve the boundary conditions when testing at the component level. In other cases, time-varying or stochastic boundary conditions may need to be simulated. Further, the impedance of components may need to be simulated in order to perform test machine calibration without risking high-value assets in the process. In cases such as these, passively shunted electromechanical transducers may be used to simulate the required mechanical impedances.

Equations required to describe the coupled electromechanical behavior of both piezoelectric and magnetostrictive transducers were derived. The interaction of both the electrical and mechanical boundary conditions must be considered when designing shunt circuits to achieve the desired impedance functions. The conditions resulting in resonance of the loaded, shunted transducer were derived and validated through experimentation.

The equations derived for predicting and tailoring the mechanical impedance of these devices were based on linear models. Although more sophisticated material models could be used, the simplifications used in this work provide reasonably accurate results for the intended applications. The use of variable inductors and capacitors in the electrical shunt can provide flexibility to provide final adjustment of the mechanical impedance to account for deviations from the predicted values. Nonlinear behavior was observed in the experiment and attributed to changes in the transduction coefficient through a stress dependence of the piezoelectric coefficient. Although not verified, it is concluded that magnetostrictive Terfenol-D transducers may behave more linearly and with less hysteresis than soft PZT.

Future work in this area will include experimental validation of the equations for magnetostrictive transducers as well as incorporation and demonstration of passively shunted transducers in actual dynamic test fixtures.

## Acknowledgements

The author wishes to acknowledge Jim Redmond, Dave Clauss for the financial support through the Engineering Sciences Research Foundation required to conduct this effort, and Dr. Todd Simmermacher for experimental support and comments, and Dr. Andrei Zagrai and Daniel Kitts of New Mexico Tech for their useful comments.

## References

[1] T.D. Scharton, Force Limited Vibration Testing Monograph. NASA Reference Publication RP-1403, 1997.
[2] T.D. Scharton, Impedance simulation vibrations test fixtures for spacecraft tests, *Shock and Vibration Bulletin* 40 (3) (1969) 230–256.
[3] R.L. Forward, Electronic damping of vibrations in optical structures, *Journal of Applied Optics* 18 (5) (1979) 690–697.
[4] N.W. Haywood, A. von Flowtow, Damping of structural vibrations with piezoelectric materials and passive electrical networks, *Journal of Sound and Vibration* 146 (2) (1991) 243–268.
[5] S.O.R. Moheimani, A.J. Fleming, *Piezoelectric Transducers for Vibration Damping and Control*, Springer, London, 2006.
[6] S.Y. Wu, Method for multiple mode shunt damping of structural vibration using a single PZT transducer *Proceedings of the SPIE Symposium on Smart Structures and Materials—Smart Structures and Intelligent Systems*, March 1998, pp. 159–167.
[7] G.S. Agnes, D.J. Inman, Nonlinear piezoelectric vibration absorbers, *Smart Materials and Structures* 5 (1996) 704–714.
[8] D.L. Hall, A.B. Flatau, Broadband performance of a magnetostrictive shaker, *Journal of Intelligent Material Systems and Structures* 6 (1) (1995) 109–116.
[9] J. Pratt, A.B. Flatau, Development and analysis of a self-sensing magnetostrictive actuator design, *Journal of Intelligent Material Systems and Structures* 6 (1995) 639–648.
[10] H. Kwun, K.A. Bartels, Magnetostrictive sensor technology and its applications, *Ultrasonics* 36 (1998) 171–178.
[11] R.C. Fenn, M.J. Gerver, Passive damping and velocity sensing using magnetostrictive transduction, *Proceedings of the SPIE Symposium on Smart Structures and Materials—Smart Structures and Intelligent Systems*, Vol. 2190, 1994, pp. 216–227.
[12] C.L. Davis, G.A. Lesieutre, An actively tuned solid-state vibration absorber using capacitive shunting of piezoelectric stiffness, *Journal of Sound and Vibration* 232 (3) (2000) 601–617.

[13] F.V. Hunt, *Electroacoustics, The Analysis of Transduction, and its Historical Background*, Acoustical Society of America, Woodbury, NY, 1982.
[14] D.A. Berlincourt, D.R. Curran, H. Jaffe, *Piezoelectric and Piezomagnetic Materials and their Function in Transducers, Physical Acoustics: Principals and Methods*, Academic Press, New York, 1964.
[15] D. Zhou, M. Kamlah, D. Munz, Effects of uniaxial prestress on the ferroelectric hysteretic response of soft PZT, *Journal of the European Ceramics Society* 25 (2005) 425–432.
[16] D. Zhou, M. Kamlah, High-field dielectric and piezoelectric performance of soft lead zirconate titanate piezoceramics under combined electromechanical loading, *Journal of Applied Physics* 96 (11) (2004).
[17] D. Zhou, M. Kamlah, D. Munz, Uniaxial compressive stress dependence of the high-field dielectric and piezoelectric performance of soft PZT piezoceramics, *Journal of Materials Research* 19 (3) (2004).
[18] J.L. Butler, *Application Manual for the Design of Etrema Terfenol-D Magnetostrictive Transducers*, EDGE Technologies, Inc., 1988.
[19] M.B. Moffett, A.E. Clark, M. Wun-Fogle, J. Linberg, J.P. Teter, E.A. McLaughlin, Characterization of Terfenol-D for magnetostrictive transducers, *Journal of the Acoustical Society of America* 89 (3) (1991).
[20] A.E. Clark, J.P. Teter, M. Wun-Fogle, Magnetomechanical coupling in Bridgman-grown $Tb_{0.3}Dy_{0.7}Fe_{1.9}$ at high drive levels, *Journal of Applied Physics* 67 (9) (1990).
[21] A.J. Fleming, S. Behrens, S.O.R. Moheimani, Synthetic impedance for implementation of piezoelectric shunt-damping circuit, *Electronic Letters* 36 (18) (2000).
[22] A.J. Fleming, S. Behrens, S.O.R. Moheimani, Optimization and implementation of multimode piezoelectric shunt damping systems, *IEEE/ASME Transactions on Mechatronics* 7 (1) (2002).
[23] Technical Manual. Measurement Specialties, Inc., P/N 1005663-1 REVB 02, 1999.
[24] M.D. Braynt, R.F. Keltie, A characterization of the linear and non-linear dynamic behavior of a practical piezoelectric actuator, part 1: measurements, *Sensors and Actuators* 9 (1986) 85–103.
[25] F.T. Calkins, M.J. Dapino, A.B. Flatau, Effect of prestress on the dynamic performance of a Terfenol-D transducer, *Proceedings of the SPIE Smart Structures and Materials*, 1997.
[26] F.T. Calkins, A.B. Flatau, Transducer based measurements of Terfenol-D material properties, *Proceedings of the SPIE Symposium on Smart Structures and Materials* #2717-67, 1996.
[27] S.-H. Lee, M.B. Ozer, T.J. Royston, Piezoceramic hysteresis in the adaptive structural vibration control problem, *Journal of Intelligent Material Systems and Structures* 13 (2002) 177.
[28] S.H. Lee, T.J. Royston, Modeling piezoelectric transducer hysteresis in the structural vibration control problem, *Journal of the Acoustical Society of America* 108 (6) (2000).
[29] D.L. Hall, A.B. Flatau, Nonlinearities, harmonics and trends in dynamic applications of Terfenol-D, *Proceedings of the SPIE* 1917 (1993) 929.
[30] T.J. Royston, B.H. Houston, Modeling and measurement of nonlinear dynamic behavior in piezoelectric ceramics with application to 1–3 composites, *Journal of the Acoustical Society of America* 104 (5) (1998).
[31] D. Fang, C. Li, Nonlinear electric-mechanical behavior of a soft PZT-51 ferroelectric ceramic, *Journal of Material Science* 34 (1999) 4001–4010.
[32] J. Fan, W.A. Stoll, C.S. Lynch, Nonlinear constitutive behavior of soft and hard PZT: experiments and modeling, *Acta Materialia* 47 (17) (1998–1999) 4415–4425.
[33] J.S. Forrester, E.H. Kisi, Ferroelastic switching in a soft lead zirconate titanate, *Journal of the European Ceramic Society* 24 (2004) 595–602.
[34] D.A. Hall, Review of nonlinearity in piezoelectric ceramics, *Journal of Material Science* 36 (2001) 4575–4601.
[35] C.V. Newcomb, I. Flinn, Improving the linearity of piezoelectric ceramic actuators, *Electronic Letters* 18 (11) (1982).
[36] S.-H. Lee, T.J. Royston, Modeling piezoceramic transducer hysteresis in the structural vibration control problem, *Journal of the Acoustical Society of America* 108 (6) (2000) 2843.
[37] T. Fett, S. Muller, D. Munz, G. Thun, Nonsymmetry in the deformation behaviour of PZT, *Journal of Material Science Letters* 17 (1998) 261–265.
[38] D. Damjanovic, Stress and frequency dependence of the direct piezoelectric effect in ferroelectric ceramics, *Journal of Applied Physics* 82 (4) (1997).
[39] F. Calkins, R. Smith, A. Flatau, Energy-based hysteresis model for magnetostrictive transducers, *IEEE Transactions on Magnetics* 36 (2) (2000).
[40] M.J. Dapino, F.T. Calkins, A.B. Flatau, On identification and analysis of fundamental issues in Terfenol-D transducer modeling, *Proceedings of the SPIE Symposium on Smart Structures and Materials*, 1998.
[41] M.J. Dapino, F.T. Calkins, A.B. Flatau, D.L Hall, Measured Terfenol-D material properties under varied applied magnetic field levels, *Proceedings of the SPIE Symposium on Smart Structures and Materials* #2717-66, February 1996.
[42] PI Ceramics, Piezoelectric ceramics catalog 〈www.piceramic.com〉.